Title	Autoignition of ethanol in a rapid compression machine
Author(s)	Mittal, Gaurav; Burke, Sinéad M.; Davies, Varun A.; Parajuli, Bikash; Metcalfe, Wayne K.; Curran, Henry J.
Publication Date	2013-12-09
Publication Information	Mittal, Gaurav, Burke, Sinéad M., Davies, Varun A., Parajuli, Bikash, Metcalfe, Wayne K., & Curran, Henry J. (2014). Autoignition of ethanol in a rapid compression machine. Combustion and Flame, 161(5), 1164-1171. doi: http://dx.doi.org/10.1016/j.combustflame.2013.11.005
Publisher	Elsevier
Link to publisher's version	http://dx.doi.org/10.1016/j.combustflame.2013.11.005
Item record	http://hdl.handle.net/10379/6112
DOI	http://dx.doi.org/10.1016/j.combustflame.2013.11.005

Autoignition of Ethanol in a Rapid Compression Machine

Gaurav Mittal[*1], Sinéad M. Burke[2], Varun Anthony Davies[1], Bikash Parajuli[1], Wayne K. Metcalfe[2], Henry J. Curran[2]

[1]*Department of Mechanical Engineering, The University of Akron, Akron, OH, USA*

[2] *Department of Chemistry, National University of Ireland, Galway, Ireland*

Ethanol is a renewable source of energy and significant attention has been directed to the development of a validated chemical kinetic mechanism for this fuel. The experimental data for the autoignition of ethanol in the low temperature range at elevated pressures is meager. In order to provide experimental data sets for mechanism validation at such conditions, the autoignition of homogeneous ethanol/oxidizer mixtures has been investigated in a rapid compression machine. Experiments cover a range of pressures (10–50 bar), temperatures (825–985 K) and equivalence ratios of 0.3–1.0. Ignition delay data is deduced from the experimental pressure traces. Under current experimental conditions of elevated pressures and low temperatures, chemistry pertaining to hydroperoxyl radicals assumes importance. A chemical kinetic mechanism that can accurately predict the autoignition characteristics of ethanol at low temperatures and elevated pressures has been developed and this mechanism is compared with other models available in the literature.

Keywords: ethanol; autoignition; rapid compression machine

[*] Corresponding author: gaurav@uakron.edu.

1. Introduction

Ethanol is a renewable source of energy and is used as a neat fuel as well as an octane enhancer and oxygenate in gasoline. Several investigations have focused on studying the chemical kinetics of ethanol combustion using laminar flames [1–4], shock tubes [5–10], flow reactors [11–13], jet-stirred reactors [14, 15] and a RCM [10]. Ethanol autoignition has been studied in shock tubes mostly at high temperatures and at pressures of less than 5 bar [5–10]. Few studies have been conducted at elevated pressures and at temperatures lower than 1000 K using shock tubes [8–10] and RCM [10]. At low temperatures and elevated pressures, $H\dot{O}_2$ radical chemistry can play a dominant role. In an RCM study of methanol autoignition at low temperatures, for instance, it was noted that the reaction of methanol with $H\dot{O}_2$ radical is critical to the prediction of ignition delays and the chemistry involving $H\dot{O}_2$ radicals is relatively poorly understood with a large uncertainty in rate parameters [16].

Cancino *et al.* [9] measured ignition delays of ethanol at $\phi = 0.3$ and 1 at temperatures in the range 770–1250 K and at pressures of 10–40 bar in a shock tube. Lee *et al.* [10] determined ignition delay times for stoichiometric ethanol mixtures at 775–1000 K and 80 bar using a shock tube and complemented these with RCM measurements at 35 bar. Autoignition at low temperatures can be influenced by phenomena that are facility specific. In shock tubes for instance, experiments at low temperatures can manifest a pressure rise due to shock attenuation. In addition, significant fuel-specific pre-ignition behavior is sometimes noted where ignition is inhomogeneous to begin with, and is followed by a pronounced deflagrative phase, compression of the unburned mixture and the eventual autoignition. In the shock tube study of Fieweger *et al.* [17], the pressure increase due to the deflagrative phase shortened the time for methanol autoignition by an order of magnitude at 800 K and 40 bar. Given the high sensitivity of

induction chemistry to perturbation from shock attenuation and deflagrative phase, such effects are accounted for in kinetic modeling [18].

By using Schlieren imaging in a shock tube, Lee *et al.* [10] also noted deflagrative behavior in ethanol autoignition. Pressure measurements as well as emission signals showed strong pre-ignition behavior with pressure increasing by more than 100% in some cases before autoignition. Ignition delays reported without any pressure histories can be highly misleading and could lead to misinterpretation of the experimental data at low temperatures. In contrast to the study of Lee *et al.* [10], Cancino *et al.* [9] did not report any pre-ignition pressure rise and adjusted the kinetic mechanism to mimic the plateau in the ignition delay profile at low temperatures. Specifically, a significantly higher value for the rate constant of the ethanol + $H\dot{O}_2$ reaction was adopted [10]. Consistent with [10], faster ignition in [9] could have been from facility dependent in-homogeneous and strong pre-ignition effects and the adjustment to the $H\dot{O}_2$ radical chemistry might be unreasonable.

On the other hand, observed ignition delays in an RCM are typically longer than in shock tubes due to post-compression heat loss. The data from an RCM is free from the pre-ignition pressure rise that is typical of mild ignition in a shock tube, and the post-compression heat loss can be satisfactorily simulated to isolate chemical kinetic effects. Since the autoignition of ethanol in an RCM has rarely been investigated, the objective of this work is to study this phenomenon and provide useful data for mechanism validation over a range of pressures and equivalence ratios. In the following, the experimental facility is first described followed by the results of the autoignition experiments and a comparison with available kinetic models as well as model refinements.

2. Experimental Specifications

Experiments were conducted in a pneumatically driven and hydraulically damped RCM. It has a compression cylinder of 5.08 cm bore and an optimized crevice design to suppress the roll-up vortex. The end combustion chamber of 4.67 cm bore is connected to the compression cylinder through a gradually converging section. This design allows 'crevice containment', where the crevice is isolated from the main reaction chamber at the end of compression, which prevents additional mass flow into the crevice when chemical heat release takes place in the main chamber. The specifications of the RCM and the details of the CFD analysis to arrive at the optimized combustion chamber configuration were presented in [19, 20]. The compression stroke can be varied between 20.32 and 30.48 cm and the clearance volume is also adjustable allowing for a range of compression ratios up to 16. The dynamic pressure during the experiment is measured using a piezoelectric sensor (Kistler 6052C) and a charge amplifier (Kistler 5010B). The test mixtures are first prepared manometrically inside a 19 L stainless steel tank equipped with a magnetic stirrer and allowed to homogenize before feeding to the combustion chamber.

Autoignition investigations for ethanol/O_2/N_2/Ar mixtures were conducted over the temperature range of 825–985 K, the pressure range of 10–50 bar, and for ϕ from 0.3 to 1. The mixture compositions and the ranges of compressed gas pressures and temperatures at the end of compression (top dead center, TDC), P_C and T_C, are given in Table 1. Dilution with N_2+Ar, required to attain an appropriate value of phi within a particular range of compressed gas temperature, was set to be in the same proportion as the non-reactive components in air. For a given mixture composition, the compressed gas temperature within each range (Table 1) was varied by altering the compression ratio, whereas the desired pressure was obtained by independently varying the initial pressure of the reacting mixture. The temperature at the TDC,

T_C, was determined by the adiabatic core hypothesis according to the relation $\int_{T_0}^{T_c} \frac{\gamma}{\gamma - 1} \frac{dT}{T} = \ln[P_c / P_0]$, where P_0 is the initial pressure, T_0 the initial temperature, γ is the specific heat ratio and is a function of temperature.

3. Results

3.1 Ignition Delay Data

An example of a primary pressure trace for autoignition is shown in Fig. 1. The measured pressure and the deduced temperature at the end of compression (t = 0) are P_C = 49.9 bar and T_C = 851 K, respectively. It is also seen from Fig. 1 that the compression stroke is ~25 ms, and the ignition delay (τ) is defined as the time from the end of the compression stroke, where the pressure peaks at t = 0, to the instant of rapid pressure rise due to ignition. In the case of relatively slower pressure rise during ignition, the inflection point in the pressure trace during ignition is taken as the instant of ignition to determine ignition delay. The corresponding non-reactive pressure trace in Fig. 1 also illustrates that the post-compression pressure decay in this RCM is moderate and pressure falls by less than 7% over a 50 ms interval. The relatively low rate of fall immediately after the piston has stopped, and its subsequent overall extent, is attributed to the stopping of mass flow into the crevice during the post compression period owing to crevice containment. It has been shown elsewhere [19] that a significantly higher of pressure decay is manifested during the initial 10s of ms after compression when crevice containment is not employed. Experimental pressure traces over a range of T_C for ϕ = 0.3 and P_C = 25 bar are shown in Fig. 2 and the pressure rise during ignition is noted to be rapid even at long ignition delays, albeit with a much slower 'burn out' in the final stage of combustion.

Figure 3 is a plot of ignition delay times from previous studies of ethanol autoignition, scaled to first order with oxygen concentration, versus the reciprocal of temperature. The present data is also included. The experimental data sets in Fig. 3 have varying fuel loading and equivalence ratio and the purpose is to emphasize the domain of the present experiments in contrast to the previous studies. A scatter in the present dataset is noted on this plot because scaling with respect to the fuel concentration is not considered here. It is evident that the data from shock tubes at low temperatures shows a plateau in the ignition delay curve, possibly due to the pre-ignition pressure rise, whereas RCM data does not show this behavior.

The compiled ignition delay times for different equivalence ratios and compressed pressures are shown in Figs. 4 and 5 as a function of the inverse compressed gas temperature, T_C.

A regression analysis is further conducted for the present ignition delay data yielding the correlations, $\tau = 3.4\times10^{-10}\ P_C^{-1.6}\ \phi^{-1.16}\ exp(25739/T_C)$ with regression correlation coefficient R^2=0.989. The correlation is plotted in Fig. 6 along with the experimental data. A comparison of the present correlation with that for methanol from [16] indicates that the activation temperatures for methanol (26864 K) is close to that for ethanol (25739 K), however methanol has ignition delays longer by a factor of ~ 5 at 25 bar in the temperature range of 800–1000 K.

3.2 Kinetic Models

Numerical modeling of experiments is performed using the Sandia SENKIN code [21] in conjunction with CHEMKIN. The modeling begins from the start of the compression stroke, and includes the effect of heat loss after the end of compression. For each reactive experiment, a non-reactive experiment with a mixture of the same specific heat was first conducted. The non-reactive pressure history is used to deduce the effective volume based on adiabatic volume

expansion. Separate polynomials are fitted to the effective volume during compression and post compression period. These fitted volume polynomials are subsequently used to simulate the experiment using SENKIN. Details of the heat transfer modeling approach are similar to [22].

The kinetic mechanisms available in the literature for ethanol [4,13,14,23,24] are primarily based on revisions to the mechanism from Marinov [24]. The mechanism presented in this work is based on the recent publication from Metcalfe *et al.* [25] who presented a C_1–C_2 sub-mechanism (Aramco Mech 1.3) validated over a large range of experimental conditions for both hydrocarbon and oxygenated species. The hydrogen/oxygen sub-mechanism has been adopted from the recent study of Kéromnès *et al.* [26]. The choice of the important rate constants for the ethanol sub-mechanism are discussed in detail in that study and will only be briefly discussed here.

Most of the development for the ethanol sub-mechanism was carried out as part of the development of the C_1–C_2 mechanism [25]. The experimental data presented in this study is at lower temperatures than previous ignition delay data and in order to match this data AramcoMech 1.3 required some refinements. The overall level of agreement between the mechanism and experimental targets presented in the Supplementary Material of [25] has been maintained and can be seen in the Supplementary Material of this study. The complete mechanism as well as a mechanism performance against other C_1–C_2 targets is available on our website http://www.nuigalway.ie/c3/Mechanism_release/frontmatter.html. The changes from Metcalfe *et al.* study are a refinement of the rate constant for the reaction of ethanol and hydroperoxyl radical and by analogy the reaction of ethanol and methyl peroxy radicals.

The performance of the mechanism presented in this study is compared to the mechanisms from Marinov [24] and Li et al. [23] in Fig. 7. An example of the modeling of experiments is

presented in Fig. 7(a). Experimental and simulated pressure traces for both the reactive mixture and the corresponding nonreactive mixture with the same heat capacity ratio are shown in Fig. 7(a). Experimental and simulated delays for P_C = 10, 25 and 50 bar, and ϕ = 0.3 are shown in Fig. 7(b). The mechanisms from Li et al. and Marinov over-predict the ignition delay by approximately 40% at 10 bar and by a factor of 2 or more at 25 and 50 bar. Previously Aramco Mech 1.3 [25] was faster than the experimental data. However, the updated mechanism presented in this study shows relatively good agreement with the experimental data presented and can accurately predict the effect of pressure and equivalence ratio on ignition delay times as seen in Figs. 4 and 5. This mechanism has been validated over a wide range of initial conditions and experimental devices including flow reactor, shock tube, a jet-stirred reactor and flame studies, and comparisons of the mechanism against these targets is included in the supplementary material. Table 2 contains the rate constants for the important reactions forming part of the ethanol oxidation sub-mechanism.

A brute-force sensitivity is included in Fig. 8 in order to highlight the important reactions at a range of equivalence ratios. This analysis involves increasing and decreasing each reaction rate expression by a factor of two and calculating the effect on the predicted ignition delay time. The sensitivity coefficient σ is defined as $\sigma = \log(\tau' / \tau'') / \log(2.0/0.5)$ where τ' is the ignition delay time calculated with the increased rate coefficient and τ'' is the ignition delay time calculated using the decreased rate expression. This definition results in negative sensitivity coefficients for reactions promoting reactivity and positive coefficients for those inhibiting reactivity. An integrated flux-analysis was conducted prior to ignition in order to give an indication of the dominant reactions taking place before ignition at 25 bar and ϕ = 0.5, shown in Fig. 9. The overall reaction proceeds primarily via $C_2H_5OH \rightarrow s\dot{C}_2H_4OH \rightarrow CH_3CHO \rightarrow CH_3\dot{C}O \rightarrow \dot{C}H_3$

→ $CH_3\dot{O}_2$ → $CH_3\dot{O}$ → CH_2O. The important reactions pertaining to ethanol autoignition are discussed next.

$C_2H_5OH+H\dot{O}_2$

Ethanol can undergo hydrogen atom abstraction from three sites. Abstraction of a hydrogen atom alpha to the hydroxyl group in ethanol leads to the formation of $CH_3\dot{C}HOH$ or $s\dot{C}_2H_4OH$ radicals, while abstraction of a hydrogen atom beta to the hydroxyl group generates $\dot{C}H_2CH_2OH$ or $p\dot{C}_2H_4OH$ radicals. Finally, abstraction of the alkoxy hydrogen atom generates ethoxy ($C_2H_5\dot{O}$) radicals.

The most sensitive reaction shown in Fig. 8 and the reaction that consumes the most fuel according to Fig. 9 is hydrogen abstraction by hydroperoxyl radical from the α-carbon on ethanol, resulting in the formation of $s\dot{C}_2H_4OH$ and hydrogen peroxide (H_2O_2) in a chain propagating reaction. The hydrogen peroxide subsequently decomposes, resulting in the formation of two reactive hydroxyl radicals in a chain branching reaction.

It is this pressure dependent reaction ($H_2O_2(+M)\Leftrightarrow \dot{O}H+ \dot{O}H(+M)$), yielding an increase in the concentration of hydroxyl radicals, that enhances the reactivity at higher pressures, as shown in Fig. 4. The main chain branching pathways generally emanate from the fuel species thus there is also an increase in reactivity when going from lean to rich mixtures in this temperature regime, as shown in Fig. 5.

The rate constants for the hydrogen abstraction reaction of ethanol with hydroperoxyl radical adopted in *this study* is an analogy with the recent study of Zhou *et al.* [27] who investigated the reaction of *n*-butanol and hydroperoxyl radical. The *A*-factor from the alpha site forming $s\dot{C}_2H_4OH$ as stated in Zhou *et al.* was increased by a factor of 1.75 which is within the stated uncertainty of a factor of 2.5. This is a smaller increase than was previously stated in Metcalfe *et*

al. [25] who increased the Zhou *et al*. recommendation by a factor of 2.5. The other channels remain unchanged from the recommendations in AramcoMech 1.3 [25].

The rate constant for the reaction of hydroperoxyl radical with ethanol from Marinov [23] is an estimated rate constant based on analogy with methanol, the Li *et al.* [24] recommendation is based on the Marinov value but includes a different branching ratio (Fig. 10(b)). Figure 10(a) compares the total rate constants from *this study*, the Marinov mechanism and the Li *et al.* mechanism. The rate constant recommended in this study is approximately 35% faster than the other two values in the temperature range of this study. Hydrogen abstraction from ethanol by methyl-peroxy radical is also highlighted in Fig. 8 as being sensitive; the rate constant for this reaction is assumed to be analogous to the hydroperoxyl radical rate constant, but the total rate constant is a factor of two lower than the $H\dot{O}_2$ recommendation. Neither the Marinov nor Li *et al.* mechanisms contain rate constants for this set of reactions. The effect of changing the rate constant of the major channel within its state uncertainty is seen in Fig. 11.

$C_2H_5OH + \dot{O}H$

Figure 9 shows that hydrogen abstraction by hydroxyl radicals consumes a significant amount of the fuel (approximately 32%). The reaction which forms $s\dot{C}_2H_4OH$ radical and water is highlighted as an inhibiting reaction in the sensitivity analysis in Fig. 8, as this chain propagating reaction competes with the chain branching reaction of $C_2H_5OH+H\dot{O}_2$. The rate constants for reactions of hydroxyl radical with ethanol have been adopted from the study of Sivaramakrishnan *et al*. [28]. The choice of rate constants is discussed in detail in our recent publication [25]. The Marinov recommendation is based on studies from Hess and Tully [29] and Bott and Cohen [29], the Li *et al.* recommendation is from the PhD thesis of Li [31]. Figure 12 compares the Sivaramakrishnan *et al*. recommendation to the rate constants in the Marinov and

Li *et al.* mechanisms. The rate constants from Marinov and Li *et al.* are lower than the value recommended in AramcoMech 1.3 by a factor of 1.75 at 1000 K, there is also a discrepancy in the branching ratio (Fig. 12(b)), while we predict that the channel forming $s\dot{C}_2H_4OH$ is dominant across the temperature range, both Marinov and Li *et al.* assign a greater importance to the channel forming the ethoxy radical. The total rate constant from Sivaramakrishnan *et al*. shows good agreement with theoretical studies from Zheng and Truhlar [32] and Xu and Lin [33].

$s\dot{C}_2H_4OH + O_2$

Although not highlighted as sensitive in the analysis in Fig. 8 the reaction $s\dot{C}_2H_4OH$ and molecular oxygen has been shown in Fig. 9 to consume almost 100% of the $s\dot{C}_2H_4OH$ formed. The $s\dot{C}_2H_4OH$ radical is consumed by reaction with molecular oxygen to give acetaldehyde and hydroperoxyl radical, the rate constant for this reaction has been adopted from a recent theoretical study by da Silva *et al*. [34] This rate constant is in good agreement with another relatively recent theoretical study from Zádor *et al.* [35] The rate constant recommend by Marinov is based on an analogy with the reaction of $\dot{C}H_2OH+O_2$, and a similar rate constant is recommended in the Li *et al.* mechanism. We have adopted from da Silva *et al*. as it provides rate coefficients applicable across a wide range of temperatures and pressures, 300–2000 K and 0.001–100 atm.

CH_3CHO

Acetaldehyde chemistry is also highlighted in Fig. 8 as being important for the combustion of ethanol at the conditions of this study and a thorough discussion of important rate constants for acetaldehyde is included in [25]. The most sensitive acetaldehyde reaction highlighted in Figs. 8 and 9 is the reaction of $CH_3CHO+H\dot{O}_2$. This further emphasizes the importance of hydroperoxyl chemistry in this temperature and pressure range. The rate constant adopted in AramcoMech 1.3

is taken from the Baulch *et al.* review [37] and the total rate constant is in good agreement with the recommendations in both the Marinov and Li *et al.* mechanisms and is within a factor of two of a recent theoretical study [38].

$H\dot{O}_2$+$H\dot{O}_2$

The sensitivity analysis also reveals $H\dot{O}_2+H\dot{O}_2<=>H_2O_2+O_2$ as an inhibiting reaction. This reaction consumes *two* $H\dot{O}_2$ radicals to generate one H_2O_2 molecule, which subsequently decomposes into two $\dot{O}H$ radicals. On the other hand, the reaction of $H\dot{O}_2$ radical with any stable species leads to the formation of one H_2O_2 molecule from *one* $H\dot{O}_2$ radical. In this case ultimately four $\dot{O}H$ radicals would be produced from two $H\dot{O}_2$ radicals and not two $\dot{O}H$ radicals that result from the $H\dot{O}_2+H\dot{O}_2$ self-reaction. The rate constant for this reaction is adopted from the study of Hippler *et al.* [39] and there is further discussion on this reaction in our recent study [26].

4. Concluding Remarks

Ignition delay time data from an RCM has been taken for ethanol at low temperatures and elevated pressures over a range of equivalence ratios. This has enabled improvement in the performance of a chemical kinetic mechanism that can accurately predict combustion characteristics of ethanol at the conditions of this study. Despite the changes that have been implemented in *this study* the mechanism performance of AramcoMech 1.3 against wide range of experimental conditions and facilities has been maintained. Sensitivity and flux analysis revealed that the most important and sensitive reactions under the present experimental conditions are those involving hydroperoxyl radicals, namely $C_2H_5OH+H\dot{O}_2$ and $CH_3CHO+H\dot{O}_2$ as well as the formation of H_2O_2 from $H\dot{O}_2$ radical and its subsequent decomposition.

Specifically, a revision in rate constants of the $C_2H_5OH+H\dot{O}_2$ reactions allowed for improved predictions and captured the effect of pressure and equivalence ratio on ignition delay times. As seen in the Supplementary Material, one issue with the current mechanism is the consistent under-prediction of ethylene concentrations across a range of conditions. A flux analysis carried out at 1 atm showed that ethylene comes from the decomposition of 1-hydroxy ethyl radical ($p\dot{C}_2H_4OH$). One possible reason for the under-prediction of ethylene is the under-production of $p\dot{C}_2H_4OH$ radical.

Comment [ISS1]: Sinead, you need to be specific here, T, p, phi?, range

Comment [ISS2]: Do you mean from the abstraction reactions and if so which radical is responsible? Is it OH?

References

1. Gülder, O., Proc. Combust. Inst. 19 (1982) 275–281.
2. Egolfopoulos, F. N., Du, D. X., Law, C. K., Proc. Combust. Inst.24 (1992) 833–841.
3. Kasper, T. S., Osswald, P., Kamphus, M., Kohse-Höinghaus, K., Combust. Flame 150 (2007) 220–231.
4. Saxena, P., Williams, F. A., Proc. Combust. Inst. 31 (2007) 1149–1156.
5. Natarajan, K., Bhaskaran, K.A., Int. Symp. Shock Waves 13 (1981) 834.
6. Dunphy, M.P., Simmie, J.M., J. Chem. Soc. Faraday Trans. 87 (1991) 1691–1696.
7. Curran, H. J., Dunphy, M. P., Simmie, J. M., Westbrook, C. K., Pitz, W. J., Proc. Combust. Inst. 24 (1992) 769–766.
8. Heufer, K., Olivier, H., Shock Waves 20 (2010) 307–316.
9. Cancino, L.R., Fikri, M., Oliveira, A.A.M., Schulz, C., Energy Fuels 24 (2010) 2830–2840.
10. Lee, C., Vranckx, S., Heufer, K.A., Khomik, S.V., Uygun, Y., Olivier, H., Fernandes, R.X., Z. Phys. Chem. 226 (2012) 1–27.
11. Li, J., Kazakov, A., Dryer, F. L., Int. J. Chem. Kinet. 33 (2001) 859–867.
12. Li, J., Kazakov, A., Dryer, F. L., J. Phys. Chem. A 108 (2004) 7671–7680.
13. Haas, F. M., Chaos, M., Dryer, F.L., Combust. Flame 156 (2009) 2346–2350.
14. Leplat, N., Dagaut, P., Togbé, C., Vandooren, J., Combust. Flame 158 (2011) 705–725.
15. Frassoldati, A., Cuoci, A., Faravelli, T., Ranzi, E., Combust. Sci. and Tech. 182 (2010) 653–667.
16. Kumar, K., Sung, C.J., Int. J. Chem. Kinet. 43 (2011) 175–184.
17. Fieweger, K., Blumenthal, R., Adomeit, G., Combust. Flame 109 (1997) 599–619.
18. Chaos, M., Dryer, F. L., Int. J. Chem. Kinet. 42 (2010) 143–150.

19. Mittal, G., Bhari, A., Combust. Flame (2013) http://dx.doi.org/10.1016/j.combustflame.2013.06.027.

20. Mittal, G., Gupta, S., Fuel 102 (2012) 536–544.

21. Lutz, A. E., Kee, R. J., Miller, J. A., SENKIN: A FORTRAN Program for Predicting Homogeneous Gas Phase Chemical Kinetics with Sensitivity Analysis. Sandia National Laboratories, Report No. SAND 87-8248, 1988.

22. Mittal, G., Sung, C.J., Combust. Sci. Tech., 2007, 179(3) 497–530.

23. J. Li, M. Chaos, A. Kazakov, F. L. Dryer, F. M. Haas, Personal communication: Ethanol Model v1.0", Princeton University, Princeton, New Jersey, December 2009.

24. Marinov, N., Int. J. Chem. Kinet. 31 (1999) 183–220.

25. Metcalfe, W. K., Burke, S. M., Ahmed, S. S., Curran, H. J, Int. J. Chem. Kin. DOI 10.1002/kin.20802.

26. Kéromnès, A., Metcalfe, W. K., Heufer, K. A., Donohoe, N., Das, A. K., Sung, C.-J., Herzler, J., Naumann, C., Griebel, P., Mathieu, O., Krejci, M. C., Petersen, E.L., Pitz, W.J., Curran, H. J., Combust. Flame 160 (2013) 995–1011.

27. Zhou, C.W., Simmie, J.M., Curran H.J., Int. J. Chem. Kin. 44 (2012) 155–164.

28. Sivaramakrishnan, R., Su, M.C., Michael, J.V, Klippenstein, S.J., Harding, L.B., Ruscic, B., J. Phys. Chem. A, (2012) 9425–9439.

29. Hess, W. P., Tully, F. P., Chem. Phys. Lett. 152 (1989) 183–189.

30. Bott, J. F., Cohen, N., Int. J. Chem. Kinet. 23 (1991) 1075–1094.

31. Li, J., PhD Thesis, Princeton University 2004.

32. Zheng, J., Truhlar, D.G., Faraday Discuss. 157 (2012) 59–88.

33. Xu, S., Lin, M. C., Proc. Combust. Inst. 31 (2007) 159–166.

34. da Silva, G., Bozzelli, J. W., Liang, L., Farrell, J. T., J. Phys. Chem. A 113 (2009) 8923–8933

35. Zádor, J., Fernandes, R. X., Georgievskii, Y., Meloni, G., Taatjes, C. A., Miller, J. A., Proc. Combust. Inst. 32 (2009) 271–277.

36. Taylor, P. H., Rahman, M. S., Arif, M., Dellinger, B., Marshall, P., Symp. Int. Comb. 26 (1996) 497–504.

37. Baulch, D. L., Cobos, C. J., Cox, R. A., Esser, C., Frank P., Just, T., Kerr, J.A., Pilling, M.J., Troe, J., Walker, R.W., Warnatz, J. J. Phys. Chem. Ref. Data 21 (1992) 411–734.

38. Altarawneh M., Al-Muhtaseb, A. A. H., Dlugogorski, B. Z., Kennedy, E. M., Mackie, J. C., J. Comp. Chem. 32 (2011) 1725–1733.

39. Hippler H., Troe J., Willner J., J. Chem. Phys. 93 (1990) 1775–1760.

Table 1 – Molar composition of test mixtures

#	ϕ	Ethanol	O_2	N_2	Ar	P_C (bar)	T_C (K)
1	0.3	1	10	8.16	29.44	10, 25, 50	825–985
2	0.5	1	6	1.72	20.84	10, 25	825–985
3	1	1	3	0	11.28	10	860–925

Table 2 – Important reactions in the ethanol sub-mechanism discussed in the text. Units: cm^3/mol/s/cal unit

Reaction	Pressure	A	n	Ea	Ref
$C_2H_5OH+(M)<=>C_2H_4+H_2O+(M)$	(1atm)	5.23E+43	–8.90	81506.7	[28]
$C_2H_5OH+(M)<=>\dot{C}H_3+\dot{C}H_2OH+(M)$	(1atm)	5.55E+64	–14.50	106183.	[28]
$C_2H_5OH+(M)<=>\dot{C}_2H_5+\dot{O}H+(M)$	(1atm)	4.46E+65	–14.90	112345.	[28]
$C_2H_5OH+\dot{H}<=>s\dot{C}_2H_4OH+H_2$		8.79E+04	2.70	2910.	[28]
$C_2H_5OH+\dot{H}<=>p\dot{C}_2H_4OH+H_2$		5.31E+04	2.81	7490.	[28]
$C_2H_5OH+\dot{H}<=>C_2H_5\dot{O}+H_2$		9.45E+02	3.14	8701.1	[28]
$C_2H_5OH+\dot{O}H<=>s\dot{C}_2H_4OH+H_2O$		7.17E+04	2.54	–1534.	[28]
$C_2H_5OH+\dot{O}H<=>p\dot{C}_2H_4OH+H_2O$		5.70E+00	3.38	–2394.3	[28]
$C_2H_5OH+\dot{O}H<=>C_2H_5\dot{O}+H_2O$		5.81E–03	4.28	–3560.	[28]
$C_2H_5OH+H\dot{O}_2<=>s\dot{C}_2H_4OH+H_2O_2$		2.45E–05	5.26	7475.1	*This Study*
$C_2H_5OH+H\dot{O}_2<=>p\dot{C}_2H_4OH+H_2O_2$		2.79E–02	4.30	15333.	*This Study*
$C_2H_5OH+H\dot{O}_2<=>C_2H_5\dot{O}+H_2O_2$		4.53E–07	5.30	10533.1	*This Study*
$C_2H_5OH+CH_3\dot{O}_2<=>s\dot{C}_2H_4OH+CH_3O_2H$		1.22E–05	5.26	7475.1	*This Study*
$C_2H_5OH+CH_3\dot{O}_2<=>p\dot{C}_2H_4OH+CH_3O_2H$		1.40E–02	4.30	15333.	*This Study*
$C_2H_5OH+CH_3\dot{O}_2<=>C_2H_5\dot{O}+CH_3O_2H$		2.21E–07	5.30	10533.1	*This Study*
$s\dot{C}_2H_4OH+O_2<=>CH_3CHO+H\dot{O}_2$	(1atm)	5.28E+17	–1.64	839.	[34]
$s\dot{C}_2H_4OH+O_2<=>C_2H_3OH+H\dot{O}_2$	(1atm)	7.62E+02	2.45	–296.	[34]
$CH_3CHO+\dot{O}H<=>CH_3\dot{C}O+H_2O$		3.37E+12	0.00	–619.	[31]
$CH_3CHO+\dot{O}H<=>HOCHO+\dot{C}H_3$		3.00E+15	–1.08	0.	[36]
$CH_3CHO+\dot{O}H<=>\dot{C}H_2CHO+H_2O$		1.72E+05	2.40	815.	[36]
$CH_3CHO+H\dot{O}_2<=>CH_3\dot{C}O+H_2O_2$		3.01E+12	0.00	11920.	[37]

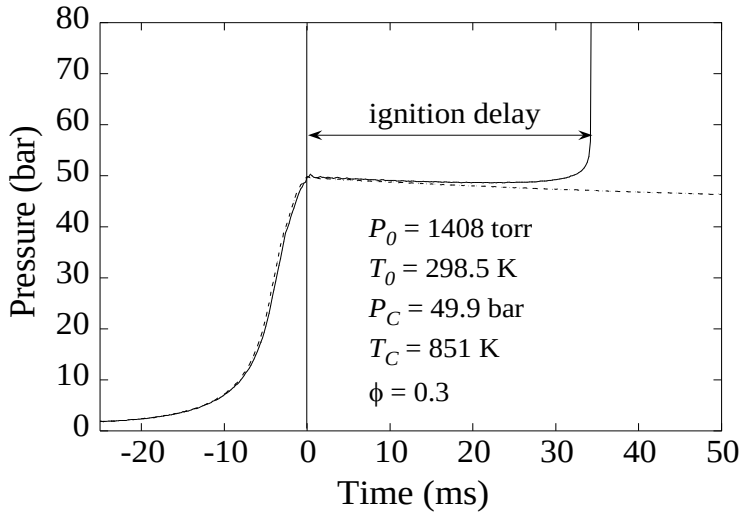

Fig. 1 –Typical experimental pressure trace and definition of ignition delay.

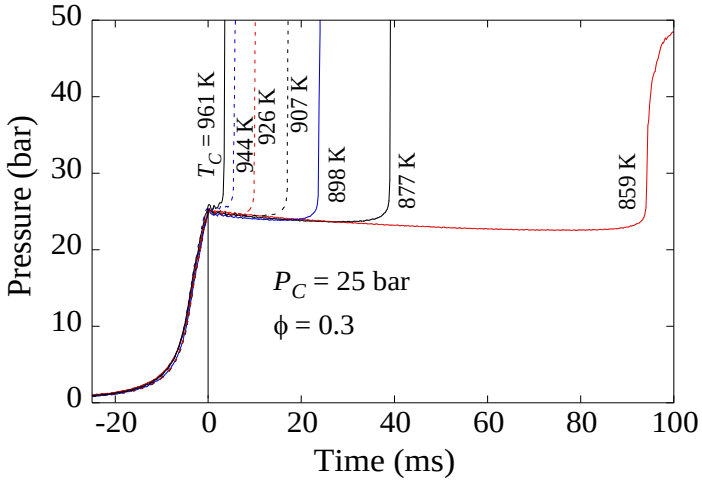

Fig. 2 – Experimental pressure traces with variation of T_C. P_C = 25 bar, ϕ =0.3

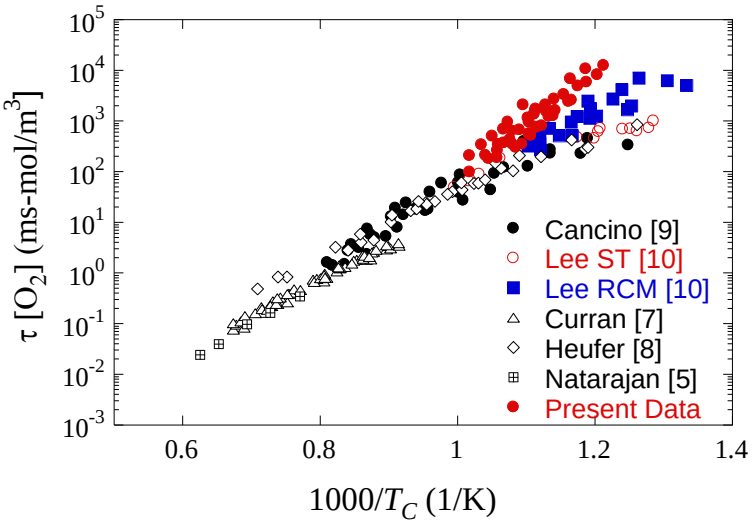

Fig. 3 – Comparison of literature data for ethanol autoignition

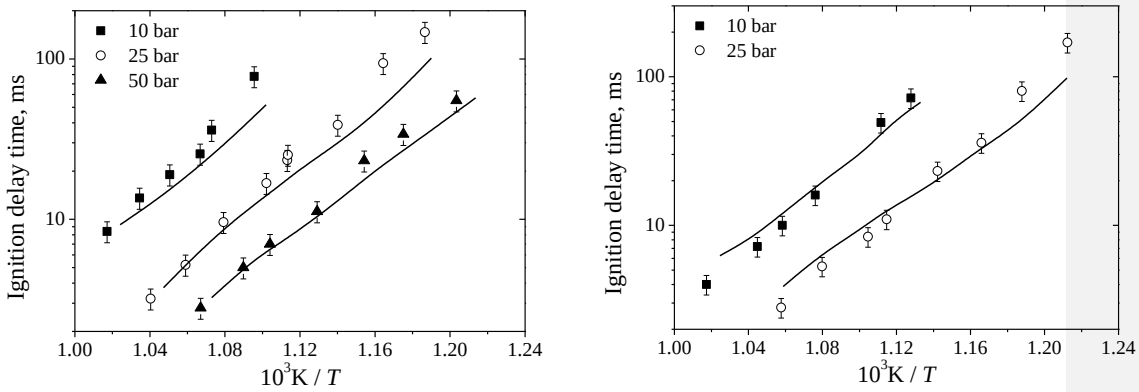

Fig. 4– Effect of pressure on ignition delay times for ϕ = 0.3 and 0.5. Symbols are experimental data while lines are model simulations.

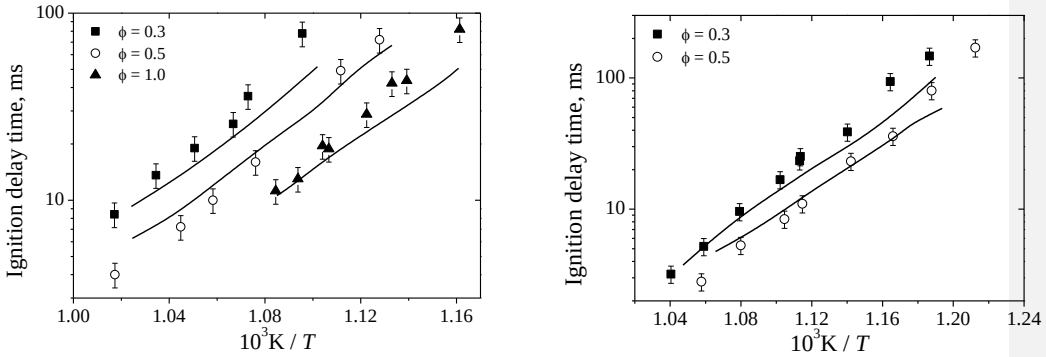

Fig. 5– Effect of equivalence ratio on ignition delay times for P_C = 10 and 25 bar. Symbols are experimental data while lines are model simulations.

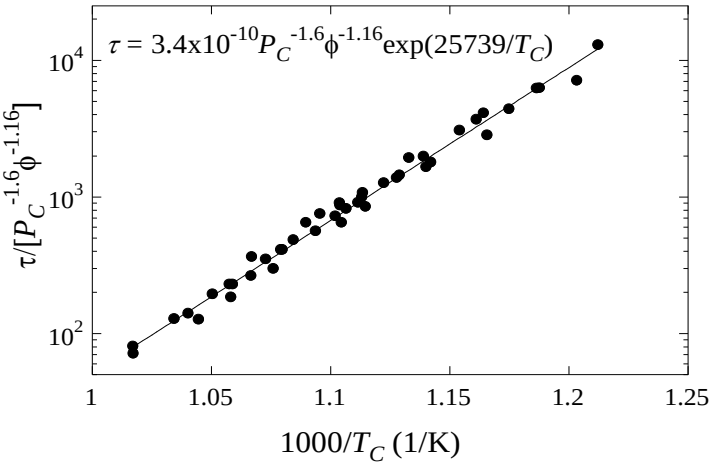

Fig. 6– Ignition delay correlation along with the experimental data

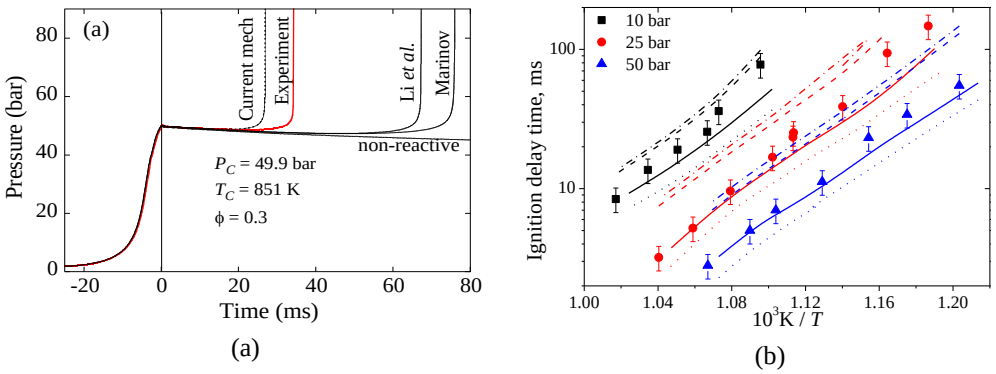

Fig. 7– Comparison of experimental data at ϕ = 0.3 with models. (b) Solid line: Current mechanism, dashed line Marinov mechanism [24], dashed dotted line Li *et al.* mechanism [23] and dotted line previous version of AramcoMech 1.3 as published in [25].

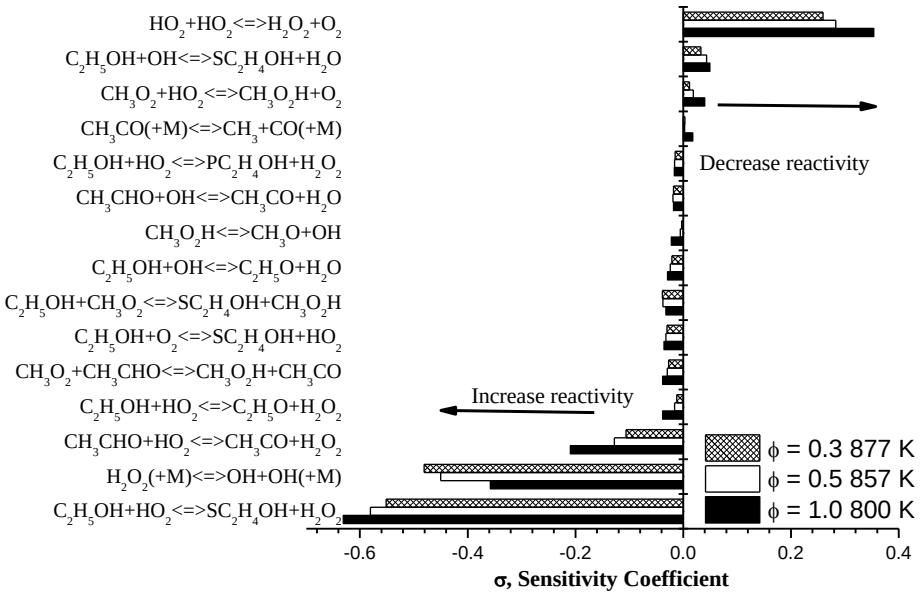

Fig. 8 - Sensitivity analysis for ignition delay time for P = 25 atm and ϕ = 0.3, 0.5 and 1.0 for approximately the same ignition delay time.

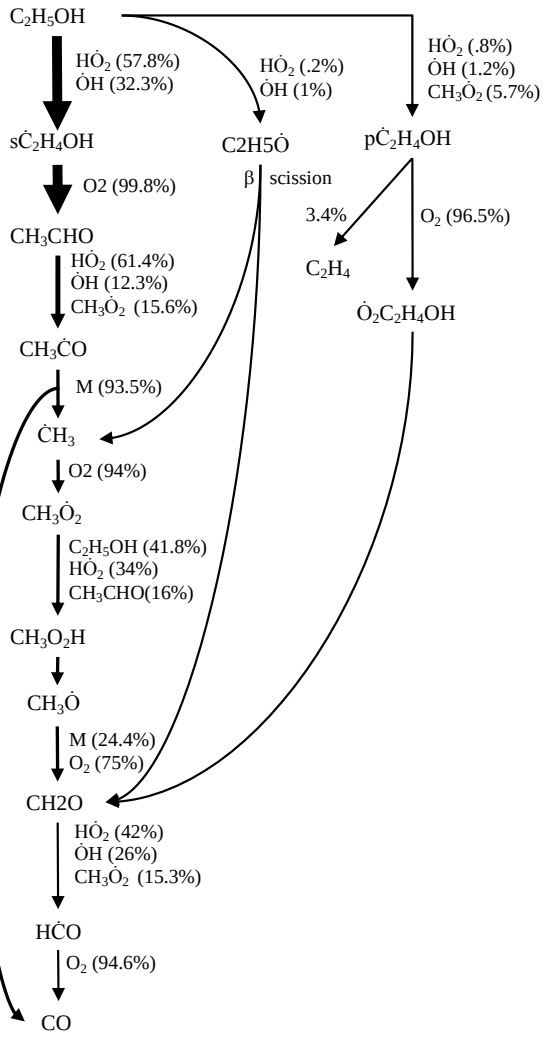

Fig. 9 – Integrated flux analysis (up to 25 K temperature rise due to pre-ignition heat release) for ethanol autoignition using the current mechanism. Molar composition - $C_2H_5OH/O_2/N_2/Ar$ = 1/6/1.72/20.84; Temperature = 800 K; Pressure = 25 atm.

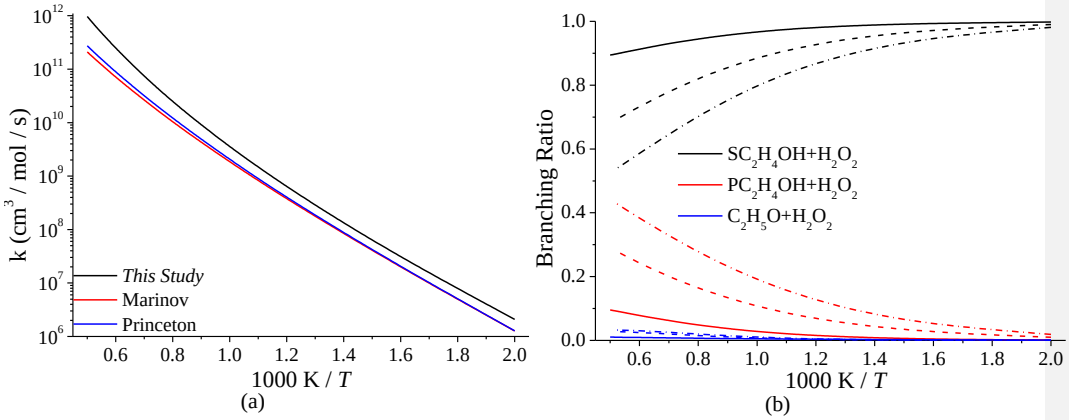

Fig. 10 – (a) Total rate constant for $C_2H_5OH+H\dot{O}_2$ from *this study*, the Marinov mechanism [24] and the Li *et al.* mechanism [23]. **(b)** Branching ratio for $C_2H_5OH+H\dot{O}_2$, solid line *this study*, dashed line the Marinov mechanism and the dash dot line the Princeton mechanism.

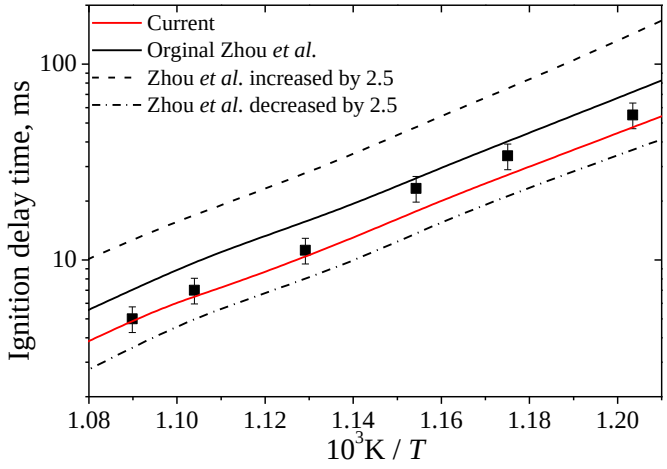

Fig. 11 - Effect of changing the rate constant for $C_2H_5OH+H\dot{O}_2$ within its stated uncertainty as described in Zhou *et al.* [27] on experimental data at ϕ = 0.3 fuel in air mixture at 50 atm

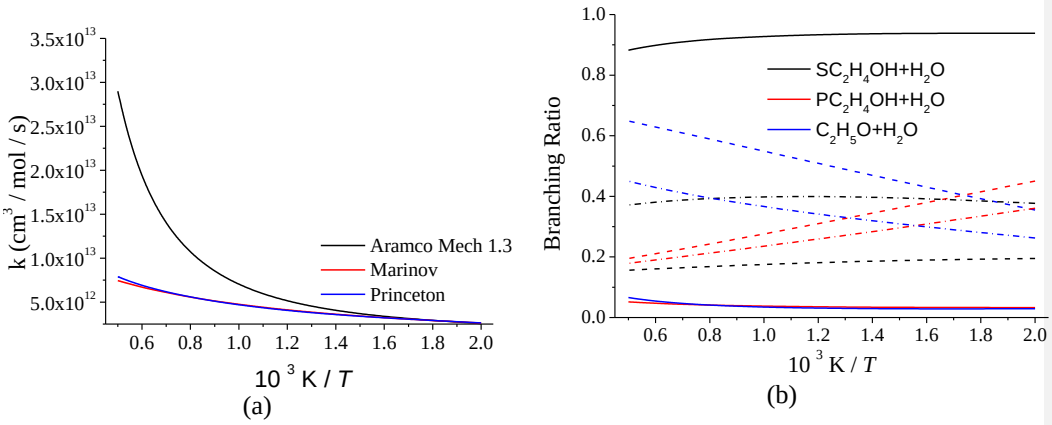

Fig. 12 – (a) Total rate constant for $C_2H_5OH+\dot{O}H$ as recommended in *this study* (AramcoMech 1.3), the Marinov mechanism and the Princeton mechanism. **(b)** Branching ratio for $C_2H_5OH+\dot{O}H$, solid line *this study* (AramcoMech 1.3), dashed line the Marinov mechanism and the dash dot line the Princeton mechanism.